Analysis of charge separation dynamics in a semiconductor junction

W. K. Metzger, R. K. Ahrenkiel, J. Dashdorj, and D. J. Friedman
National Renewable Energy Laboratory, Golden, Colorado 80401, USA
(Received 18 April 2004; revised manuscript received 30 September 2004; published 3 January 2005)

Charge separation has been experimentally observed in a number of junction devices over the last decade, but there has been little theoretical analysis of the phenomena that describes the detailed dynamics of the effect. In this work, we use computer simulations to assess the ability of time-resolved photoluminescence, resonant-coupled photoconductive decay, and other experimental techniques to characterize free-carrier recombination and charge separation after an ultrafast laser pulse excites carriers in a homojunction or a heterojunction. The results indicate the experimental conditions where charge separation is likely to dominate these measurements and several experimental signatures that can be used to distinguish charge separation from free-carrier recombination. Time-resolved photoluminescence and resonant-coupled photoconductive decay measurements on Si, $GaAs/Ga_xIn_{1-x}P$, and other junctions confirm and illustrate the results.

DOI: 10.1103/PhysRevB.71.035301 PACS number(s): 78.47.+p, 72.40.+w

I. INTRODUCTION

Semiconductor and nanoscience technology is dependent on our ability to understand and manipulate transport and recombination processes in microstructures. Techniques designed to observe carrier kinetics and recombination, such as time-resolved photoluminescence (TRPL), resonant-coupled photoconductive decay (RCPCD), and transient transmission, are critical tools in accomplishing this. The traditional and most straightforward way to characterize recombination in semiconductor materials is to inject excess carriers into confinement devices such as a double heterostructure. Optical excitation is produced with a fast laser pulse, and one observes the subsequent decay in photoluminescence, photoconductivity, or any other physical property related to the excess carrier density. The confinement limits excess carriers to the material under investigation, simplifies analysis, and can help control surface recombination.[1]

Measurements of recombination in the presence of a charge-separating field are more difficult to interpret. The field sweeps excess carriers and quickly alters the spatial profiles of the excess electrons and holes, thereby distorting recombination rates and making analysis complex. Nonetheless, the emergence of ultrafast laser technology has stimulated numerous experimental TRPL and photoconductivity decay (PCD) studies to characterize the presence and rate of charge separation in diverse materials such as superlattices, blended acceptor-donor polymers, semiconductor-liquid interfaces, quantum structures, conjugated-polymer/semiconductor-nanocrystal composites, and ordered/disordered III-V and III-V:N semiconductors.[2–14]

The extension of TRPL and PCD experiments to characterize bulk recombination, rather than charge-separation, in completed semiconductor devices with charge-separating fields is both lacking and needed. Completed devices may have recombination properties due to interface, material, and growth issues that cannot be observed in double heterostructures or other test configurations. For example, CdTe solar cells are generally grown by depositing thin layers of tin oxide (TO) and polycrystalline CdS (100 nm) on a glass substrate, followed by a layer of polycrystalline CdTe.[15] Currently, no method can create a confining double heterostructure for studying recombination in either polycrystalline CdS or CdTe. Even when recombination in polycrystalline CdTe and CdS can be characterized independently, it may not be all that relevant, because recombination at the highly lattice-mismatched CdS/CdTe interface may dominate device performance. In spite of the many experimental studies of charge separation in diverse systems, there is not enough theoretical work to know if and under what conditions TRPL or RCPCD measurements on a semiconductor homojunction or heterojunction can give meaningful values of the underlying bulk recombination rates.

The problem of electron-hole dynamics in the presence of a charge-separating field following a short laser pulse generally does not have an analytical solution. So early analytical treatments focused on low-injection conditions and replaced the field in homojunction devices with a surface recombination or excess-carrier boundary condition, thereby failing to capture the full role of the junction on recombination under diverse experimental conditions.[16–18] Rosenwaks *et al.* published results detailing the impact of electron-hole dynamics on TRPL spectra for a semiconductor layer placed between a larger-band-gap confining semiconductor layer on one side, and air, solution, or another confinement layer on the other.[19] Recent computer modeling has focused on depleted surface layers and semiconductor-liquid interfaces.[6,20,21]

The computer simulations that we present here are designed to describe how an internal field, charge separation, and diffusion affect RCPCD, TRPL, and other lifetime measurements on complete *p-n* homojunction and heterojunction devices. This understanding allows us to specify the signatures of charge separation in lifetime measurements and the conditions under which recombination or charge separation are likely to dominate the decay signal. Although the simulations and experimental data are specific to bulk heterojunctions and homojunctions, the results provide some insights about charge separation and lifetime measurements in other material systems.

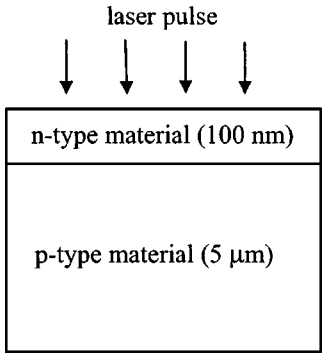

FIG. 1. Schematic of the generic device structure used for the simulations.

II. NUMERICAL SIMULATIONS

In each simulation, a 500-fs Gaussian laser pulse injects carriers into either a n/p junction (see Fig. 1) with a 100 -nm n-type emitter and a 5-μm p-type base, or a homogenous 5.1-μm layer of p-type material. During and after the laser pulse, excess electrons and holes recombine, diffuse, and drift simultaneously within the sample. Thermalization occurs on a much faster time scale than these processes for the materials and physical parameters considered, and the effect of self-heating is negligible. Consequently, hydrodynamic equations are not necessary, and carrier transport is modeled using a drift-diffusion model, where the governing equations are given by the following forms of the Poisson and continuity equations:

$$\nabla \cdot \mathbf{E} = \frac{q}{\varepsilon}(p - n + N_d - N_a), \tag{1}$$

$$\nabla \cdot \mathbf{J}_p = \nabla \cdot (q\mu_p p\mathbf{E} - qD_p \nabla p) = q\left(G - R - \frac{\partial p}{\partial t}\right), \tag{2}$$

$$\nabla \cdot \mathbf{J}_n = \nabla \cdot (q\mu_n n\mathbf{E} + qD_n \nabla n) = -q\left(G - R - \frac{\partial n}{\partial t}\right). \tag{3}$$

Here, q is the elementary electronic charge, ε is the electrical permittivity, n and p are the total free electron and hole densities, N_d and N_a are the ionized donor and acceptor concentrations, $\mathbf{J}_p$ and $\mathbf{J}_n$ represent the hole and electron current densities due to drift and diffusion, $\mathbf{E}$ is the electric field, D_p and D_n are the hole and electron diffusion coefficients, and μ_p and μ_n are the hole and electron mobilities, respectively. G describes the generation rate due to the laser pulse and is proportional to

$$\alpha I(t)e^{-\alpha z}, \tag{4}$$

where I is the intensity of the laser pulse, α is the coefficient of absorption, and z is the depth into the sample relative to the plane of incidence. Photoinjection is uniform in the plane parallel to the surface of the sample. R describes the total recombination rate, which we have set equal to the sum of the rate of radiative recombination and Shockley-Read-Hall (SRH) recombination. The radiative recombination rate per unit volume, R_{rad}, is given by

$$R_{rad}(t) = B[p(\mathbf{r},t)n(\mathbf{r},t) - p_0(\mathbf{r})n_0(\mathbf{r})], \tag{5}$$

where B is the radiative coefficient, and p_0 and n_0 are the equilibrium hole and electron concentrations, respectively. The SRH recombination rate per unit volume, R_{SRH}, is modeled with the classic equation[1]

$$R_{SRH}(t) = \frac{p(\mathbf{r},t)n(\mathbf{r},t) - p_0(\mathbf{r})n_0(\mathbf{r})}{\tau_p(\mathbf{r},t)[n(\mathbf{r},t) + n_i(\mathbf{r})e^{(E_t - E_i)/kT}] + \tau_n(\mathbf{r},t)[p(\mathbf{r},t) + n_i(\mathbf{r})e^{(E_i - E_t)/kT}]}, \tag{6}$$

where n_i represents the intrinsic carrier density, E_t represents the energy level of a single trap, E_i represents the intrinsic Fermi energy level, and τ_p and τ_n represent the hole and electron SRH lifetimes, respectively. To make the role of the junction on lifetime measurements as transparent as possible, we simplified the interpretation by assuming minimal free-surface recombination, setting E_t equal to E_i, and making τ_p and τ_n equal and constant throughout the sample for most simulations. So, from here forward, we will write τ_p and τ_n as τ_{SRH} and refer to them simply as the SRH lifetime.

The layer materials, carrier concentrations, injection level, laser wavelength, and material parameters were varied to understand how photoconductivity and photoluminescence decay signals are altered by the presence of the junction in diverse conditions. Experimentally, the optical properties of a sample and photon recycling can affect RCPCD and TRPL decay curves.[1] A full computation of these phenomena is extremely difficult and cumbersome. Here, we calculate the photoconductivity signal,σ_{ph}, from the equation

$$\sigma_{ph}(t) = q\int_V d^3\mathbf{r}[\mu_n(\mathbf{r},t)\Delta n(\mathbf{r},t) + \mu_p(\mathbf{r},t)\Delta p(\mathbf{r},t)], \tag{7}$$

and the PL intensity at a given time by integrating the radiative recombination rate over the volume of the sample. This approach leaves out any dependence on the external experimental configuration, but also excludes the role of optical issues such as internal absorption and photon recycling. Upon analyzing the results and inspecting recombination versus position, it is clear that these exclusions do not significantly alter the results or conclusions to be presented.

A numerical solution was obtained with the device simulator DESSIS from Integrated Systems Engineering, Inc., which uses the finite-difference method. Equations (1)–(3) were discretized using box discretization and the backward Euler method.[22,23] Saturation of the free-carrier drift velocity due to high electric fields was accounted for using a saturation velocity of 7.7×10^6 cm/s. Variation of the mobility with doping for GaAs was accounted for using appropriate parameters in the model described by Arora *et al.*[24]

III. RESULTS AND DISCUSSION

Numerous thin-film semiconductor materials, including GaAs, InGaAs, InGaAsP, GaAsN, InGaAsN, GaInN, GaNP, CdTe, and $Cu(In,Ga)Se_2$, typically have recombination lifetimes in the range of 100 ps to 10 μs.[15,25–31] If lifetime measurements on junction devices using these materials are any indication of underlying recombination rates, the decay curves should at least vary with the lifetime values assigned to the underlying materials. In our first four simulations, we model a GaAs homojunction and assign a SRH lifetime value of 100 ps, 1 ns, 10 ns, or 100 ns throughout the entire sample. The radiative recombination coefficient for GaAs, 2×10^{-10} cm^3/s, is typical of III-V semiconductors.[30] So, for the simulations presented here, the overall lifetime is determined largely by the SRH lifetime. The low-field, low-carrier-concentration electron and hole mobilities are 8000 and 350 $cm^2/V\,s$, respectively, and in these conditions, the majority and minority carrier mobilities are taken to be equal. The electron and hole diffusion coefficients are calculated from the corresponding mobilities using the Einstein relation. The absorption coefficient, 4.8 μm^{-1}, corresponds to an excitation wavelength of 600 nm.[32] The effective electron and hole masses are $0.067m_0$ and $0.48m_0$, respectively, where m_0 is the mass of a free electron. The injection level was varied over many orders of magnitude. For easy reference, we will define P_0 as the injection level that corresponds to 8.8×10^{11} photons/cm^2 incident on the sample after front-surface reflection.

Figure 2 illustrates the PCD and PL decay curves calculated for a GaAs homojunction with $n_0=1\times10^{17}$ cm^{-3} and $p_0=1\times10^{15}$ cm^{-3} in the emitter and the base, respectively, and a depletion width approximately 1.5 μm wide in equilibrium. At an injection level of $0.01P_0$, the PCD and the PL curves are unchanged for samples with recombination rates that vary over three orders of magnitude. So it is clear that in low injection, these measurements cannot measure carrier recombination. But at an injection level of $10P_0$, the PCD and PL decay curves do reflect the underlying recombination rates in the samples.

But it is not clear to what degree the decay curves are distorted by the junction at different injection levels and how the results extend to junctions with different doping levels. In a second set of simulations, we fix the SRH lifetime throughout the junction to 10 ns, set $n_0=1\times10^{18}$ cm^{-3} and $p_0=1\times10^{16}$ cm^{-3} in the emitter and the base, respectively, and vary the injection level by factors of 10 from $0.01P_0$ to $100P_0$. The effect of the junction is made apparent by comparing the results to corresponding simulations on a homogeneous layer of *p*-type GaAs with $p_0=1\times10^{16}$ cm^{-3}, which is an ideal lifetime test structure. Figure 3 shows that at $100P_0$, the junction has virtually no visible effect on the decay curves. At $10P_0$, which corresponds to a uniform distribution that is roughly equal to the base equilibrium hole concentration, the initial transient of the PL decay curve is altered, but overall, the decay curves are still not heavily affected by the junction. At P_0, the decay curves become marginal indicators of recombination. At lower injection levels, the PCD signal remains nearly constant for times much longer than the bulk lifetime, and the PL intensity is quenched on a time scale much faster than the bulk lifetime.

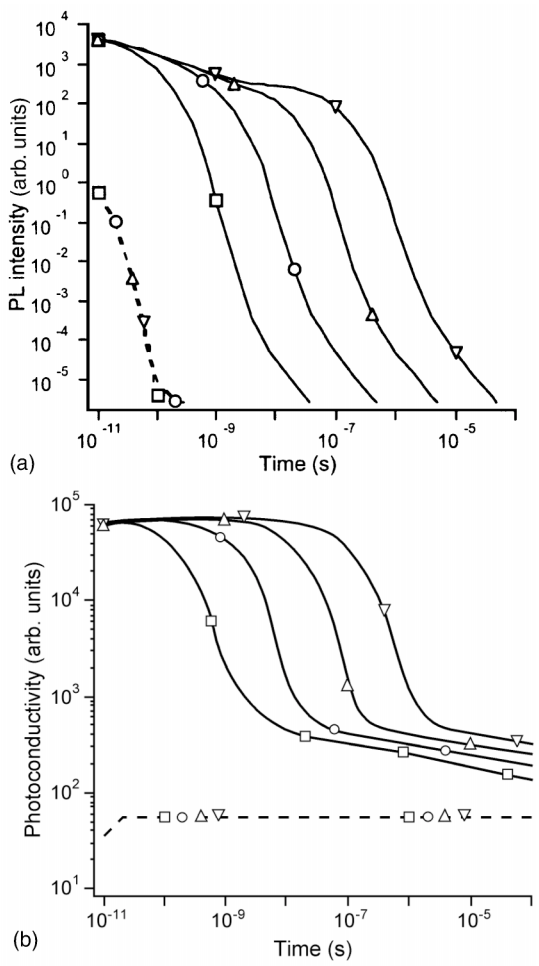

FIG. 2. PL and PCD decay curves for injection levels of $10P_0$ (solid lines) and $0.01P_0$ (dotted lines) on a GaAs junction with $n_0=10^{17}$ cm^{-3} and $p_0=10^{15}$ cm^{-3}. The square, circle, triangle, and gradient symbols represent $\tau_{SRH}=100$ ps, 1 ns, 10 ns, and 100 ns, respectively.

Figures 4 and 5 illustrate the excess electron and hole spatial distributions at distinct points in time to show the underlying physics giving rise to the observed decay curves. In low injection, immediately after the laser pulse, some excess electrons and holes have already been separated by the junction to opposite edges of the depletion region. Afterwards, some excess electrons and holes continue to be swept across the junction to the opposing depletion edge, while others diffuse deeper into the base region. Careful inspection

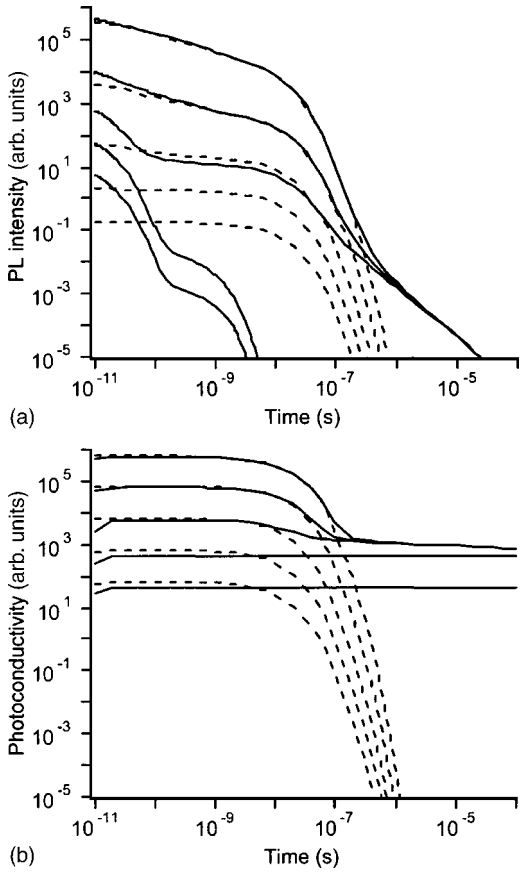

FIG. 3. PL and PCD decay curves for injection levels of 0.01, 0.1, 1.0, 10, and $100P_0$. As the injection level increases, the PL and PCD signals increase. The solid lines correspond to the GaAs junction with $\tau_{SRH}=10$ ns, $n_0=10^{18}$ cm^{-3}, and $p_0=10^{16}$ cm^{-3}. The dashed lines correspond to a layer of GaAs without a junction, where $\tau_{SRH}=10$ ns and $p_0=10^{16}$ cm^{-3}.

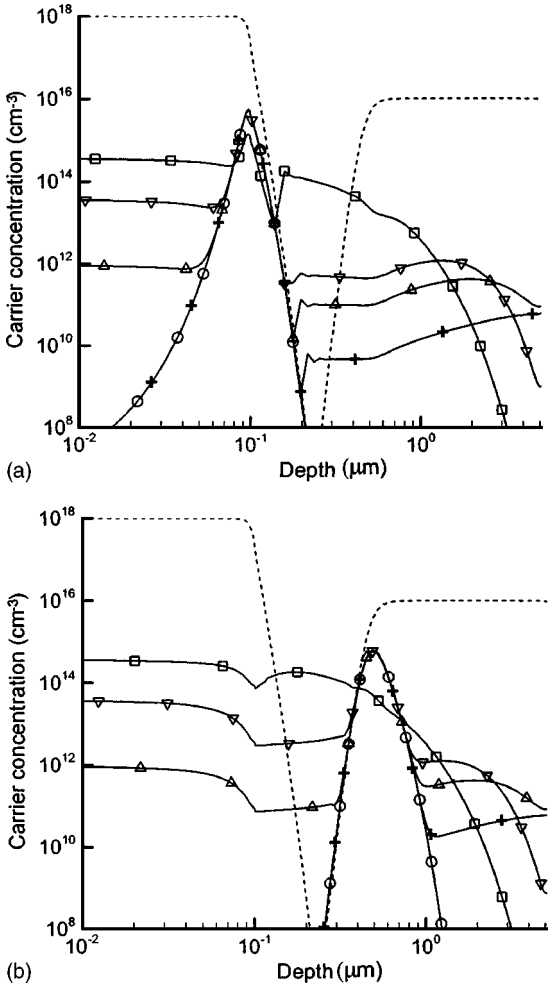

FIG. 4. Excess (a) electrons and (b) holes vs time and position for an injection level of $0.01P_0$ into a GaAs homojunction with $\tau_{SRH}=10$ ns, $n_0=10^{18}$ cm^{-3}, and $p_0=10^{16}$ cm^{-3}. The solid lines with the square, gradient, triangle, plus, and circle symbols represent the carrier distributions 0 ps, 30 ps, 90 ps, 1 ns, and 10 ms after the laser pulse, respectively. The dashed lines represent the equilibrium electron and hole concentrations.

of Fig. 4(b) shows that just 1 ns after the pulse, long before bulk recombination is prevalent, the majority of the excess holes have accumulated in the base edge of the depletion layer.

We will look at recombination at the base edge of the depletion edge and deeper into the base. Substituting $p=p_0+\Delta p$ and $n=n_0+\Delta n$ into Eq. (5) gives

$$R_{rad}(t) = B[p_0(\mathbf{r})\Delta n(\mathbf{r},t) + n_0(\mathbf{r})\Delta p(\mathbf{r},t) + \Delta p(\mathbf{r},t)\Delta n(\mathbf{r},t)]. \tag{8}$$

The product $n_0\Delta p$ in this region is much smaller than the other terms and can be neglected so that Eq. (8) becomes

$$R_{rad}(t) = B[p_0(\mathbf{r}) + \Delta p(\mathbf{r},t)]\Delta n(\mathbf{r},t). \tag{9}$$

A similar analysis of Eq. (6) indicates that the SRH rate of recombination gives

$$R_{SRH}(t) = \frac{\Delta n(\mathbf{r},t)}{\tau_{SRH}}. \tag{10}$$

So, both SRH and radiative recombination are proportional to the excess-electron density in this region. Consequently, as excess electrons are swept out of the base, as shown in Fig. 4(b), both radiative and SRH recombination fall precipitously, and excess holes in the base become long lived. A similar process occurs in the emitter region. As a result, techniques that measure a signal proportional to the total excess-carrier density, such as transient absorption and PCD, show a very slow decay that defies realistic bulk recombination lifetimes. On the other hand, TRPL and any other technique that measures a signal that is proportional to the *rate* of recombination—rather than the number of excess carriers—will have a very fast decay curve that reflects the removal of minority carriers by charge separation and not bulk recombination.

In high injection, the photoinjected carriers drastically alter the carrier concentrations and distort the equilibrium electric fields. The electric field due to the junction is still present, but has been significantly reduced in magnitude and spatial extent by the excess carriers. Throughout the junction, diffusion is the dominant transport mechanism, and excess holes are nearly equal to excess electrons. As carriers diffuse

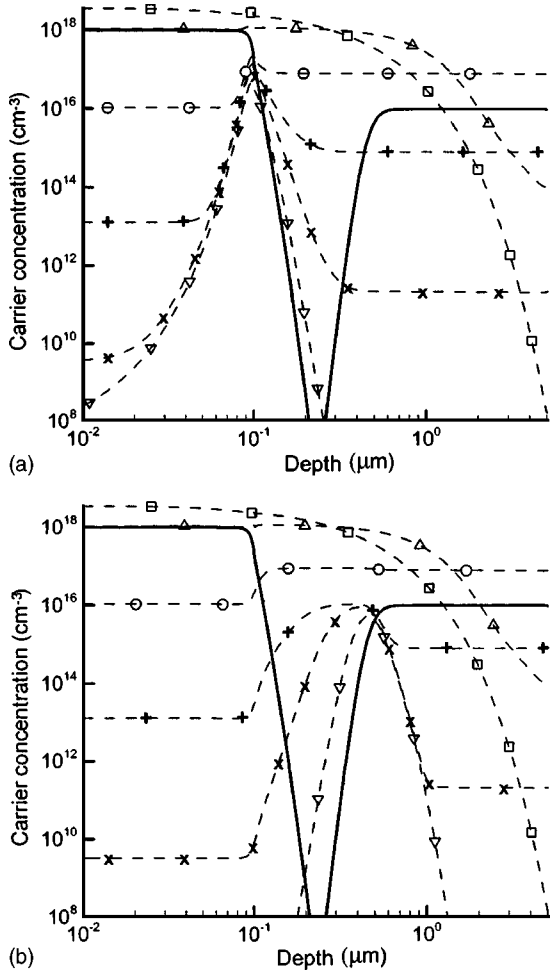

FIG. 5. Excess (a) electrons and (b) holes vs time and position for an injection level of $100P_0$ into a GaAs homojunction with $\tau_{SRH}=10$ ns, $n_0=10^{18}$ cm^{-3}, and $p_0=10^{16}$ cm^{-3}. The dashed lines with the square, triangle, circle, plus, cross, and gradient symbols represent the carrier distributions 0 ps, 90 ps, 10 ns, 100 ns, 1 μs, and 10 ms after the laser pulse, respectively. The solid lines represent the equilibrium electron and hole concentrations.

into the base, the excess-carrier concentrations around the junction decrease, and the electric field regains some magnitude and width. But even 10 ns after the pulse, the degree of charge separation is small (Fig. 5), and the number of excess electrons is nearly equal to the number of excess holes throughout the sample. Because the SRH lifetime is set at 10 ns, and the radiative lifetime is roughly 5 ns in the emitter, minority carriers begin to recombine in significant numbers about 10 ns after the pulse. As recombination continues, the junction field recovers size and spatial extent and begins to separate some charge. This can be seen clearly 100 ns after the pulse. However, throughout much of the sample, the excess electron and hole densities are still nearly equal, and the rate of minority carriers removed by charge separation is still small relative to recombination. Figure 3 indicates that 1 μs after the high-injection pulse recombination rates do become distorted by the influence of the nearly completely recovered junction field on the balance of majority and minority carriers. However, this region is beyond the dynamic

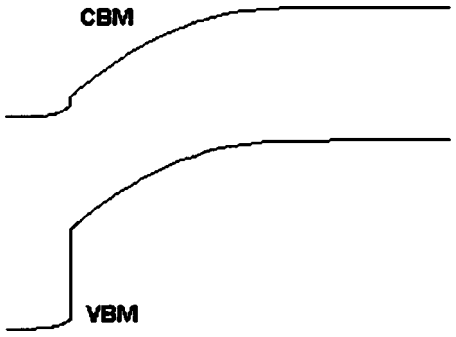

FIG. 6. Band diagram for a simple type-II heterostructure. CBM is the conduction-band minimum; VBM is the valence-band maximum.

range of most lifetime measurements, and bulk recombination has dominated most of the PCD and PL decay signals. Therefore, high-injection lifetime measurements in the presence of a junction will generally characterize the recombination properties of the underlying materials. The emitter is generally small in spatial extent, and as minority carriers recombine there, the junction limits the diffusion of more minority carriers into the region; consequently, the emitter will generally contribute only a small portion of the decay signal. Figure 3 indicates this, as do identical simulations except that the GaAs homojunction has SRH lifetimes of 100 ps in the emitter and 10 ns in the base. Figure 5 illustrates that contrary to its name, the depletion region will actually have a substantial number of excess carriers in high injection at early times. This implies that recombination in the depletion region and at the interface will contribute to experimental decay curves.

Heterojunctions have junction properties and band bending that are determined not only by the carrier concentrations, but also by intrinsic material properties. However, for a simple type-II heterojunction, such as that indicated in Fig. 6, the effect of the junction on lifetime measurements is qualitatively the same as it is for homojunctions in both low and high injection. As an example, we model a CdTe/CdS heterojunction assuming a band diagram similar to that shown in Fig. 6. The emitter parameters are $E_g=2.4$ eV, $\mu_h=25$ cm^2/V s, $\mu_n=100$ cm^2/V s, $n_0=1\times10^{17}$ cm^{-3}, $\tau_{SRH}=100$ ns, $B=2\times10^{-10}$ cm^3 s, and $\chi=4.5$ eV, where χ is the electron affinity. The base parameters are $E_g=1.5$ eV, $\mu_h=40$ cm^2/V s, $\mu_n=320$ cm^2/V s, $p_0=2\times10^{14}$ cm^{-3}, $\tau_{SRH}=100$ ns, $B=2\times10^{-10}$ cm^3 s, and $\chi=4.4$ eV. These parameters are based primarily on the material properties of CdTe and CdS,[42] but the lifetime has been made much larger for illustrative purposes. The simulations allowed for current contributions from thermionic emission and tunneling. Figure 7 indicates the PL decay curves from two different excitation wavelengths, 600 and 830 nm, that are transparent in the emitter and correspond to absorption coefficients of 5.0 and 0.36 μm^{-1} in the base, respectively. For comparison, the PL decay curve for a single 5.1-μm layer of the base material is shown, as well. A typical TRPL experiment would tune to only one emission wavelength using a monochromator, so here we include only the PL emitted from the base in the PL decay curves. In high injection, the 830-nm exci-

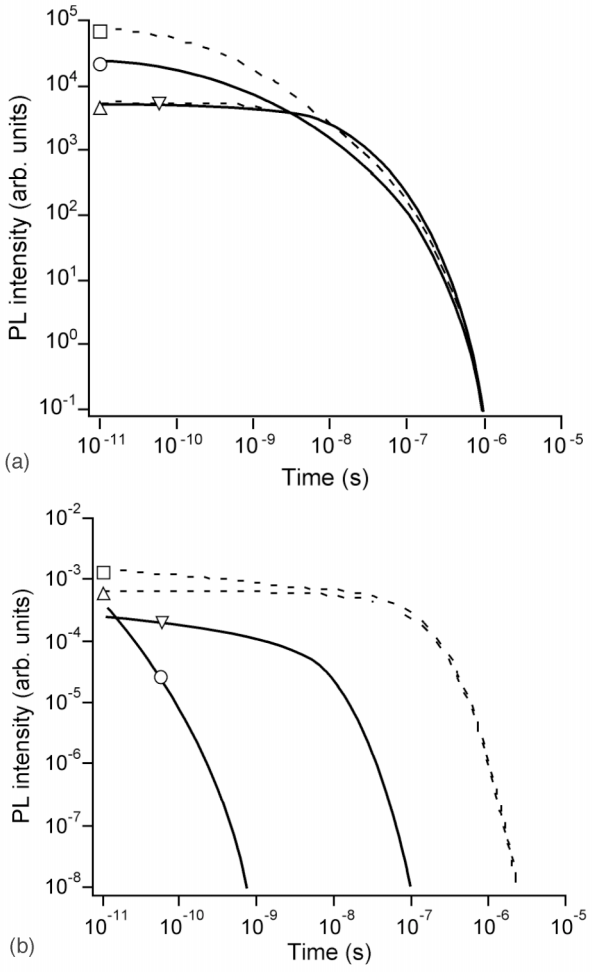

FIG. 7. PL decay curves for injection levels of $100P_0$ (a) and $0.01P_0$ (b) on the heterojunction described in the text with $\tau_{SRH}=100$ ns. The square and circle symbols correspond to an excitation wavelength of 600 nm, the triangle and the gradient symbols correspond to 830 nm. The solid lines correspond to a heterostructure, whereas the dashed lines correspond to a single layer of the 1.5 -eV material with $p_0=2\times10^{14}$ cm^{-3} throughout.

tation gives identical PL decay curves. At 600 nm, the penetration depth is much shorter, so both carrier diffusion and high-injection effects give rise to early decay transients that are not observed at 830 nm. The junction sweeps more minority carriers to the emitter region where PL is not detected, so the overall PL signal is less for the junction at 600 nm than the single layer. However, the shapes of the decay curves are very similar. In low injection, the decay curves at 600 and 830 nm are nearly the same and correctly reflect bulk recombination. The junction, once again, shows a fast decay curve that indicates charge separation rather than recombination. At 600 nm, carriers are generated near the junction, creating a much more favorable carrier distribution for fast charge separation relative to the more uniform initial distribution generated at 830 nm. Consequently, the PL intensity is quenched much more quickly at the shorter excitation wavelength. PCD decay curves show little dependence on excitation wavelength in low injection, because the mobilities in the emitter and the base are of similar magnitude, and the PCD signal is sensitive to the number of excess carriers throughout the sample, not recombination rates.

IV. CASE STUDIES

The simulations focused on just two material systems, but the trends and concepts apply to a broad range of semiconductor materials and interfaces and can lead to new physical insights in diverse contexts. A few examples will be given here.

The band alignment of $Ga_xIn_{1-x}P/GaAs$ heterostructures has attracted enormous interest due to numerous device applications. However, measured values for the conduction band offset, defined as $\Delta E_c=E_c(Ga_xIn_{1-x}P)-E_c(GaAs)$, range from 30 to 390 meV for $x\sim0.5$.[33] Outside of intrinsic experimental limitations, some of the experimental scatter may be due to the spontaneous ordering frequently observed in $Ga_xIn_{1-x}P$ and other III-V alloys. By varying growth conditions, the Ga and In atoms can form ordered arrangements on the lattice, the most common being a spontaneously generated monolayer superlattice with alternating Ga-rich and In-rich layers of $Ga_{x+\eta/2}In_{1-x-\eta/2}P$ and $Ga_{x-\eta/2}In_{1-x+\eta/2}P$, respectively, along one of the [111] directions, where η is the order parameter and varies from 0 to $\min[2x,(1-x)]$.

The spontaneous ordering has been reported to reduce the $Ga_xIn_{1-x}P$ band gap, alter the band offsets, and form polarization fields.[33–35] Within the $Ga_xIn_{1-x}P$ material, microdomains can form, creating potential fluctuations in the $Ga_xIn_{1-x}P$ layer and a very complex $Ga_xIn_{1-x}P/GaAs$ interface that is difficult to model.

To analyze the effects of ordering on lifetime measurement, isotype $Ga_{0.52}In_{0.48}P/GaAs/Ga_{0.52}In_{0.48}P$ double heterostructures were grown by metalorganic chemical vapor deposition at 650 and 750 °C on undoped GaAs substrates miscut 2° toward ⟨110⟩ from ⟨100⟩. The $Ga_{0.52}In_{0.48}P$ and GaAs double heterostructure layers were 0.05 and 2 μm thick, respectively. The $Ga_{0.52}In_{0.48}P$ PL peaks at 4 K were at 1.89 and 1.99 eV for the samples grown at 650 and 750 °C, respectively, indicating that samples grown at 750 °C had little or no ordering (d), whereas the sample grown at 750 °C had considerable ordering (o).[35]

Time-resolved photoluminescence measurements were performed at room temperature using the single-photon counting technique.[36] Excitation was provided by a mode-locked cavity-dumped dye laser firing pulses at a repetition rate set between 40 kHz and 1 MHz, at a wavelength of 580 nm, and with a beam diameter of roughly 1 mm. The photoluminescence was passed through appropriate long-pass filters and a spectrometer to a photomultiplier tube. The overall time resolution was about 30 ps. Room-temperature RCPCD measurements[37] were performed with an excitation wavelength of 750 nm with a pulse rate of 20 Hz using an optical parametric oscillator (OPO) driven by a tripled yttrium aluminum garnet (YAG) laser. The RCPCD time resolution was similar to the pulse width of the laser system, roughly 5 ns.

Figure 8 shows typical behavior for a d-$Ga_{0.52}In_{0.48}P/GaAs/d$-$Ga_{0.52}In_{0.48}P$ double heterostructure. The low-injection TRPL and RCPCD measurements give

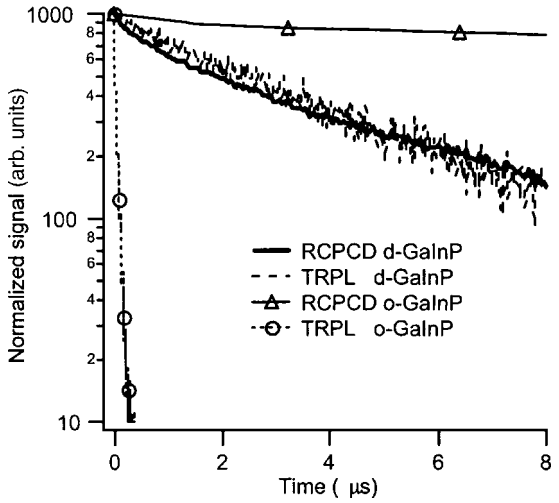

FIG. 8. RCPCD and TRPL decay curves for a *d*-$Ga_xIn_{1-x}P/GaAs/$*d*-$Ga_xIn_{1-x}P$ double heterostrucure and an *o*-$Ga_xIn_{1-x}P/GaAs/$*o*-$Ga_xIn_{1-x}P$ heterostrucure.

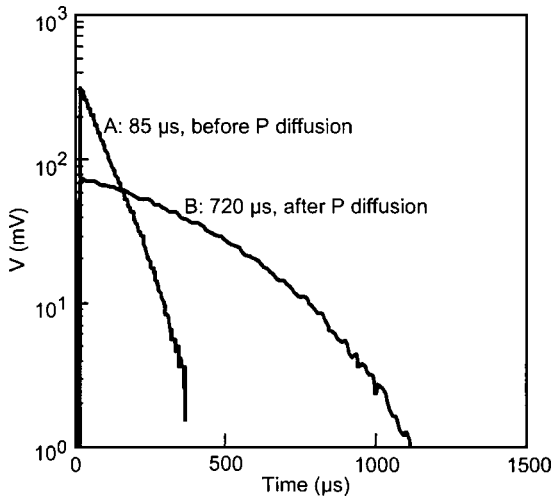

FIG. 9. RCPCD decay before and after a junction is formed by phosphorus diffusion.

nearly identical results and are accurate assessments of the recombination in the GaAs region. This is expected for a type-I alignment between the $Ga_xIn_{1-x}P$ and the GaAs. This disordered sample was lightly doped, and the long lifetime, 4.7 μs, manifests excellent material quality.

For a type-II band alignment, the simulations predict that in low-injection conditions the PL decay will be very fast, and the PCD decay will be very slow. Figure 8 shows the decay curves for the ordered sample. The PL decay is very fast, on the order of 1 ns, while the RCPCD is very slow, on the order of 1 ms. The measurements clearly indicate that the ordering of the $Ga_xIn_{1-x}P$ has shifted the band alignment from type I to type II, and that the two techniques are no longer measuring the recombination lifetime. A more in-depth study could be used to track the crossover from type-I to type-II alignment as a function of order parameter, domain size, alloy composition, and growth conditions. These results give one example of how the trends and concepts from the simulations can be applied to elucidate complex interface physics.

Another example stems from the observation that phosphorus diffusion on *p*-type Czochralski-grown single-crystalline Si wafers can increase the lifetime measured by RCPCD on the Si wafers by more than an order of magnitude (single-crystalline Si generally cannot be measured using TRPL). An initial explanation was that defects that are fast recombination centers are gettered or removed during the diffusion process and perhaps by the phosphorus near the surface. However, the simulation results indicate that a *p-n* junction formed by the phosphorus diffusion could increase the measured lifetime because of charge separation and not reflect true changes in the recombination lifetime.

To experimentally determine which of these theories was correct, lifetime was measured by the RCPCD technique using an excitation wavelength of 1000 nm on a high-quality 10 Ω cm *p*-type Si wafer. After the wafer was cleaned with HF acid and immersed in an iodine/methonal solution to reduce the surface recombination to very low values,[38] the lifetime was 85 μs. Phosphorus was then diffused into the wafer and the lifetime was measured again. As expected, the lifetime increased to 722 μs (Fig. 9). Next, the phosphorus layer was etched away and the lifetime was remeasured. If the phosphorus diffusion had truly eliminated or gettered defects, the lifetime would remain long. However, if charge separation had increased the observed lifetime, and there was no real change in the recombination rates of the Si material, the lifetime would return to near its original value. The lifetime did return to its original value (not shown), indicating that charge separation was the primary reason why the measured lifetime had increased, and that no lifetime improvement could be attributed to the phosphorus diffusion process.

It was stated in the introduction that CdTe solar cells are generally grown by depositing thin layers of tin oxide and polycrystalline CdS (100 nm) on a glass substrate, followed by a layer of polycrystalline CdTe.[15] Currently, no method can create a confining double heterostructure for studying recombination in either polycrystalline CdS or CdTe, and RCPCD measurements cannot resolve the decay times, on the order of 1 ns, generally seen in this material. Consequently, researchers have forged ahead and measured PL decay curves on completed CdTe/CdS junctions. However, interpreting the TRPL results has always been impeded by not knowing the role of the junction on the measurements. But CdTe is weakly doped, with free hole concentrations on the order of 10^{14} to 10^{15} cm^{-3}. Consequently, reaching high-injection conditions, where the simulation results predict that recombination will dominate TRPL decay curves, is not difficult. In fact, we did a recent survey and found that the decay times measured with high-injection TRPL measurements on more than 80 different CdTe/CdS samples are strongly correlated with open-circuit voltage in a mathematical form consistent with recombination lifetimes and device physics models.[15] Consequently, provided measurements are done in high injection, future studies can begin to address how recombination is affected by the many complex processes that occur both in the bulk and at the interface of CdTe and CdS.

There is currently debate about the role of grain boundaries in polycrystalline thin films.[39] Potentials due to defect

charges at grain boundaries may form charge separating junctions. In addition to separating charge, these potentials can exclude one carrier type, and the grain boundary can form a low-recombination current channel for either holes or electrons.[40,41] By measuring RCPCD and TRPL signals, and varying injection levels, it may be possible to characterize grain boundary potentials and their ability to separate charge. For *p-n* junctions in general, study of the long PCD decay after charge separation may offer a means to characterize junction leakage currents. These examples should give a feel for the diverse physical situations where the simulation results can be applied and provide new insights.

V. CONCLUSIONS

The simulations indicate both the conditions under which recombination and charge separation dominate lifetime measurements on a junction and the experimental signatures of these processes. In low injection, lifetime measurements are dominated by charge separation. As a result, PL decay is very fast, PCD decay is very slow, and the two experiments produce very different results. As the injection level is increased, lifetime measurements become dominated by recombination, and the decay times associated with the two techniques converge. The PL decay time may show a dramatic increase as the injection level is increased, whereas the PCD decay may show a dramatic decrease. In the presence of charge separation, the observed TRPL lifetime can increase dramatically as the wavelength is pushed toward the band edge, whereas the PCD decay curve will change very little provided the mobilities in the emitter and the base are of similar magnitude.

Although lifetime measurements are distorted and complicated by the presence of a junction, they can provide meaningful information about both charge-separation kinetics and recombination, provided the experimental conditions are correct. This is critical for characterizing interfaces, surfaces, and junctions that feature important physical processes that cannot be readily observed in simple test configurations such as double heterostructures.

ACKNOWLEDGMENTS

The authors would like to thank Yong Zhang for helpful discussions.

[1] *Minority Carriers in III-V Semiconductors: Physics and Applications*, edited by R. K. Ahrenkiel and M. S. Lundstrom (Academic, San Diego, CA, 1993), Chap. 2.
[2] R. Ranganathan, M. Gal, J. M. Viner, P. C. Taylor, J. S. Yuan, and G. B. Stringfellow, in *Proceedings of the 18th International Conference on the Physics of Semiconductors*, edited by O. Engström (World Scientific, Singapore, 1987), p. 763.
[3] G. Yu and A. J. Heeger, J. Appl. Phys. **78**, 4510 (1995).
[4] C. A. Leatherdale, C. R. Kagan, N. Y. Morgan, S. A. Empedocles, M. A. Kastner, and M. G. Bawendi, Phys. Rev. B **62**, 2669 (2000).
[5] Y. Gu, M. D. Sturge, K. Kash, N. Watkins, B. P. Van der Gaag, A. S. Gozdz, L. T. Florez, and J. P. Harbison, Appl. Phys. Lett. **70**, 1733 (1997).
[6] P. Schelling and J. W. Halley, Phys. Rev. B **64**, 045326 (2001).
[7] J. Cheng, S. Wang, X. Y. Li, Y. Yan, S. Yang, C. L. Yang, J. N. Wang, and W. K. Ge, Chem. Phys. Lett. **333**, 375 (2001).
[8] N. C. Greenham, S. Peng, and A. P. Alivisatos, Phys. Rev. B **54**, 17 628 (1996).
[9] Yu D. Glinka, T. V. Shahbazyan, I. E. Perakis, N. H. Tolk, X. Liu, Y. Sasaki, and J. K. Furdyna, Appl. Phys. Lett. **81**, 3717 (2002).
[10] N. A. Anderson, E. Hao, X. Ai, G. Hastings, and T. Lian, Chem. Phys. Lett. **347**, 304 (2001).
[11] R. K. Ahrenkiel, S. P. Ahrenkiel, D. J. Arent, and J. M. Olson, Appl. Phys. Lett. **70**, 756 (1997).
[12] R. K. Ahrenkiel, S. W. Johnston, B. M. Keyes, D. J. Friedman, and S. M. Vernon, Appl. Phys. Lett. **77**, 3794 (2000).
[13] S. W. Johnston, R. K. Ahrenkiel, C. W. Tu, and Y. G. Hong, J. Vac. Sci. Technol. A **21**, 1765 (2003).
[14] S. P. Ahrenkiel, S. W. Johnston, R. K. Ahrenkiel, D. J. Arent, M. C. Hanna, and M. W. Wanlass, Appl. Phys. Lett. **74**, 3534 (1999).
[15] W. K. Metzger, D. Albin, D. Levi, P. Sheldon, X. Li, B. M. Keyes, and R. K. Ahrenkiel, J. Appl. Phys. **94**, 3549 (2003).
[16] R. K. Ahrenkiel, J. Appl. Phys. **62**, 2937 (1987).
[17] S. R. Dhariwal and D. R. Mehrotra, Solid-State Electron. **88**, 1355 (1988).
[18] A. Ehrhardt, W. Wettling, and A. Bett, Appl. Phys. A: Solids Surf. **53**, 123 (1991).
[19] Y. Rosenwaks, B. R. Thacker, R. K. Ahrenkiel, A. J. Nozik, and I. Yavneh, Phys. Rev. B **50**, 1746 (1994).
[20] V. L. Malevich, Surf. Sci. **454**, 1074 (2000).
[21] S. J. Anz, O. Kruger, N. S. Lewis, and H. Gajewski, J. Phys. Chem. B **102**, 5625 (1998).
[22] R. S. Varga, *Matrix Iterative Analysis* (Springer-Verlag, New York, 2000).
[23] S. Selberherr, *Analysis and Simulation of Semiconductor Devices* (Springer-Verlag, New York, 1984).
[24] N. D. Arora, J. R. Hauser, and D. J. Roulston, IEEE Trans. Electron Devices **ED-29**, 292, 1982.
[25] S. Kurtz, J. F. Geisz, B. M. Keyes, W. K. Metzger, D. J. Friedman, J. M. Olson, A. J. Ptak, R. R. King, and N. H. Karam, Appl. Phys. Lett. **82**, 2634 (2003).
[26] A. J. Ptak, S. W. Johnston, S. Kurtz, D. J. Friedman, and W. K. Metzger, J. Cryst. Growth **251**, 392 (2003).
[27] J. F. Geisz, R. C. Reedy, B. M. Keyes, and W. K. Metzger, J. Cryst. Growth **259**, 223 (2003).
[28] B. M. Keyes, P. Dippo, W. K. Metzger, J. Abusham, and R. Noufi, J. Appl. Phys. **94**, 5584 (2003).
[29] J. Wu, W. Walukiewicz, K. M. Yu, W. Shan, J. W. Ager III, E. E. Haller, H. Lu, W. J. Schaff, W. K. Metzger, and S. Kurtz, J. Appl. Phys. **94**, 6477 (2003).
[30] *Properties of Gallium Arsenide*, edited by M. R. Brozel and G. E. Stillman (INSPEC, London, 1996).

[31] R. K. Ahrenkiel, R. Ellingson, S. Johnston, and M. Wanlass, Appl. Phys. Lett. **72**, 3470 (1998).
[32] E. D. Palik, *Handbook of Optical Constants of Solids* (Academic Press, San Diego, 1985), p. 503.
[33] Y. Zhang and A. Mascarenhas, and L. Wang, Appl. Phys. Lett. **80**, 3111 (2002).
[34] S. Froyen, A. Zunger, and A. Mascarenhas, Appl. Phys. Lett. **68**, 2852 (1996).
[35] Y. Zhang, A. Mascarenhas, and L. W. Wang, Phys. Rev. B **63**, 201312(R) (2001).
[36] D. V. O'Connor and D. Phillips, *Time Correlated Single Photon Counting* (Academic Press, San Diego, 1984).
[37] R. K. Ahrenkiel and S. W. Johnston, Mater. Sci. Eng., B **102**, 161 (2003).
[38] H. M. Saad, G. J. Norga, J. Michel, and L. C. Kimmerling, AIP Conf. Proc. **306**, 471 (1994).
[39] C. Persson and A. Zunger, Phys. Rev. Lett. **91**, 266401 (2003).
[40] I. Visoly-Fisher, S. R. Cohen, and D. Cahen, Appl. Phys. Lett. **82**, 556 (2003).
[41] C. S. Jiang, R. Noufi, J. A. AbuShama, K. Ramanathan, J. R. Moutinho, J. Pankow, and M. M. Al-Jassim, Appl. Phys. Lett. **84**, 3477 (2004).
[42] M. Gloeckler, A. L. Fahrenbruch, and J. R. Sites, in *Proceedings of 3rd World Conference on Photovoltaic Energy Conversion* (2003), p. 491.